Group Velocity Engineering of Confined Ultrafast Magnons

Y.-J. Chen,[1,*] Kh. Zakeri,[2,1,†] A. Ernst,[1,4] H. J. Qin,[1] Y. Meng,[1] and J. Kirschner[1,3]
[1]Max-Planck-Institut für Mikrostrukturphysik, Weinberg 2, 06120 Halle, Germany
[2]Heisenberg Spin-dynamics Group, Physikalisches Institut, Karlsruhe Institute of Technology, Wolfgang-Gaede-Strasse 1, D-76131 Karlsruhe, Germany
[3]Institut für Physik, Martin-Luther-Universität Halle-Wittenberg, Von-Seckendorff-Platz 1, 06120 Halle, Germany
[4]Institute for Theroretical Physics, Johannes Kepler University, Altenberger Straße 69, 4040 Linz, Austria
(Received 20 April 2017; published 27 December 2017)

Quantum confinement permits the existence of multiple terahertz magnon modes in atomically engineered ultrathin magnetic films and multilayers. By means of spin-polarized high-resolution electron energy-loss spectroscopy, we report on the direct experimental detection of all exchange-dominated terahertz confined magnon modes in a 3 ML Co film. We demonstrate that, by tuning the structural and magnetic properties of the Co film, through its epitaxial growth on different surfaces, e.g., Ir(001), Cu(001), and Pt(111), one can achieve entirely different in-plane magnon dispersions, characterized by positive and negative group velocities. Our first-principles calculations show that spin-dependent many-body correlation effects in Co films play an important role in the determination of the energies of confined magnon modes. Our results suggest a pathway towards the engineering of the group velocity of confined ultrafast magnons.

DOI: 10.1103/PhysRevLett.119.267201

One of the most pressing needs for information technology is to fabricate faster, smaller, and lower power-consumption circuits. For appealing future devices, it has been proposed to utilize bosonic quasiparticles, such as magnons, for information processing [1–3]. Furthermore, the mutual conversion between magnons and different subsystems, such as electrons [4,5], photons [6], and plasmons [7,8], opens new opportunities to realize tunable and multifunctional logic devices.

The energies of magnons span several orders of magnitude in the range from μeV to a few tenths of eV. Their wavelengths (frequencies) vary from micrometers (gigahertz) to nanometers (terahertz), governed by the weak long-range magnetic dipole-dipole interaction and the strong short-range exchange interaction, respectively. It has been demonstrated that information can be encoded in the phase or amplitude of dipolar magnons in the gigahertz regime [9–13]. However, the relevant control parameters for miniaturized magnonic circuits in the terahertz regime and on subnanometer length scales have not yet been achieved. For this purpose, ultrathin ferromagnetic films serve as ideal templates. The vertical confinement in an ultrathin film, with a thickness of a few atomic layers, eliminates the formation of long-wavelength magnons dominated by the dipolar interaction. Therefore, only short-wavelength confined magnon modes governed by exchange interaction can exist in such a structure.

In an atomically flat film, the number of confined exchange magnon modes is equal to the number of atomic layers [14]. Each magnon mode with the quantum number n has its own dispersion relation as a function of $q_{\parallel}$ over the whole surface Brillouin zone. Moreover, the atomic bonding environment for atoms at surface, interior, and interface layers is entirely different due to the presence of the vacuum-film and substrate-film interfaces. These differences result in distinctive types of terahertz magnons (surface, interior, and interface magnons) with their own characteristics [15]. As terahertz confined magnon modes are governed by the exchange interaction, modifications of the inter- and intralayer exchange constants, via tuning the lattice strain, atomic structure, or the substrate material, offer versatile tools for engineering these magnon modes.

In this Letter we report, for the first time, on the direct observation of all confined terahertz magnon modes excited in a 3 ML itinerant ferromagnetic film. Specifically, we demonstrate that, by tuning the structural and magnetic properties of the film, the propagation direction of the highest frequency confined magnon mode can be reversed, expressed by the sign change of the group velocity. Our results provide evidence that the propagation properties of all magnon modes are strongly influenced by the details of the layer-dependent exchange constants. We show that spin-dependent many-body correlations lead to a considerable reduction of the magnetic exchange interaction and a substantial energy renormalization of the confined magnon modes.

In an ultrathin film, the translational symmetry is broken in the out-of-plane direction. This leads to discrete magnon states with a quantized out-of-plane wave vector $q_{\perp} = n\pi/d$, where d is the film thickness and n is the quantum number. Figure 1 shows a "snapshot" of the confined magnon modes with quantum number $n = 0$, 1, and 2 in a three-atomic-layer ferromagnetic film. The $n = 0$ mode indicates the coherent spin precession, whereas the $n = 1$ and $n = 2$ modes correspond to one and two nodes inside the film,

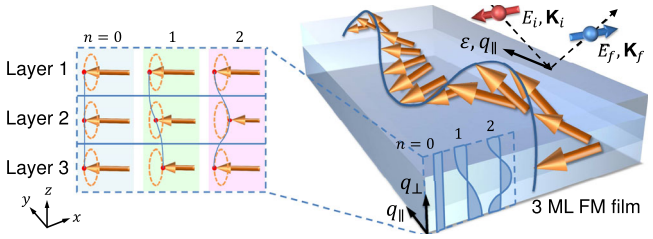

FIG. 1. Schematic representation of all three confined magnon modes with quantum numbers $n = 0$, 1, and 2, excited in a 3 ML freestanding ferromagnetic film with identical boundary conditions on top and bottom. The modes $n = 0$, 1, and 2 correspond to zero, one, and two nodes of standing spin waves with a quantized wave vector $q_\perp = n\pi/d$ and an in-plane wave vector $q_\parallel$. E_i, $\mathbf{K}_i$ and E_f, $\mathbf{K_f}$ denote the energy and wave vector of the incident and scattered electrons in spin-polarized high-resolution electron energy-loss spectroscopy (SPEELS) experiments.

respectively. This means that modes with zero, one, and two half-wavelength envelopes of standing spin waves are spanned inside the film. In consequence, spins between adjacent layers are no longer aligned parallel, and the higher energy modes are characterized by a larger deviation of the precession phase between adjacent layers. We note that, in a real film on a substrate, the presence of the substrate breaks the central symmetry of the film and the magnon modes in the film are no longer symmetric with respect to the central layer [16].

The presence of the confined magnon modes with $q_\parallel = 0$ has been reported by means of scanning tunneling spectroscopy [14,17]. High-resolution electron energy-loss spectroscopy experiments on Co films have also shown the presence of the low-energy confined magnon modes (mainly with $n = 1$) near the center of the Brillouin zone [18–22]. In addition, such confined magnons propagate in the x-y plane due to the translation invariance in the film plane. Therefore, each magnon mode has its own in-plane dispersion relation as a function of $q_\parallel$. However, the dispersion relation of all confined exchange magnon modes in a ferromagnetic film over the whole surface Brillouin zone has not yet been measured.

SPEELS permits the spin-, energy-, and momentum-resolved measurement of magnetic excitations over the whole surface Brillouin zone of low-dimensional magnets [23,24]. In the SPEELS experiments the intensity of the inelastically scattered electrons is recorded for incident electrons of opposite spin polarization, denoted as I_- and I_+. All of the information regarding energies and lifetimes of the magnons is obtained by analyzing the difference spectra $I_- - I_+$ [23–26]. Figure 2(a) shows typical SPEELS difference spectra recorded on 3 ML Co/Cu(001) with $q_\parallel$ ranging from -0.3 to -0.7 Å^{-1} along the $\bar{\Gamma}$-$\bar{X}$ direction. I_- and I_+ spectra refer to a spin polarization vector of the incoming electron beam being parallel and antiparallel to the Co$[1\bar{1}0]$ easy axis direction, respectively. In order to obtain the magnon dispersion of all modes, the difference spectra are fitted by three Lorenzian line shapes, corresponding to the magnon modes with $n = 0$, 1, and 2. The fitting procedure is carried out iteratively by nonlinear parameter optimization according to Marquardt [27]. The dispersion relation is constructed by plotting the energy of each mode versus $q_\parallel$. As presented in Fig. 2(a), the magnon peak width broadens when the mode number increases. Consequently, the high-energy modes ($n = 1$, 2) possess a much shorter lifetime than the acoustic mode ($n = 0$). This is due to the fact that the high-energy magnons live in the region of larger density of incoherent Stoner excitations and hence suffer from a larger Landau damping [16].

The dispersion relation of the confined magnon modes is determined by the strength of the exchange coupling constants in each atomic layer. In order to change these quantities, we have grown the same Co film on two additional substrates, having different lattice parameters, i.e., Ir(001) and Pt(111). Growing the film on substrates with negative and positive lattice mismatch induces compressive and tensile epitaxial stress in the film. The corresponding modification of the inter- and intralayer exchange constants has a direct consequence on the dispersion of the magnon modes.

Growth, structural, and magnetic properties of ultrathin Co films on Ir(001) [29,30], Cu(001) [31,32], and Pt(111) [33] are well known in the literature and were also verified in our experiments [34]. The film thickness and layer-by-layer growth are monitored by medium energy electron diffraction during film deposition. The magnetic properties of all Co films are investigated with the longitudinal magneto-optic Kerr effect and by SPEELS experiments. For Co/Ir(001) and Co/Cu(001), the easy magnetization axis lies along the Co$[1\bar{1}0]$ direction, while, for 3 ML Co/Pt(111), the easy magnetization axis is out of plane, in agreement with Refs. [30,32,33].

The measured dispersion relation of all three magnon modes in a 3 ML Co film on Cu(001), Ir(001), and Pt(111) is depicted as open symbols in Figs. 2(b)–2(d). Notably, in contrast to the well-known"parabolic" dispersion curve observed for the $n = 0$ magnon mode, the confined $n = 2$ magnon mode shows a "downward parabolic," "flat," and "upward parabolic" shape for Co/Ir(001), Co/Cu(001), and Co/Pt(111), respectively. This demonstrates that the dispersion relation of the confined magnon modes is extremely sensitive to small changes in the lattice structure as a result of the film epitaxy.

In order to understand the behavior of the confined magnon modes, we performed first-principles calculations within the generalized gradient approximation of the density functional theory (DFT) [35]. We used a self-consistent Green's function method, designed for semi-infinite layered structures [36]. Calculations were performed with structural parameters taken from the available experimental data for 3 ML Co/Ir(001) [29], Co/Cu(001) [37], and Co/Pt(111)

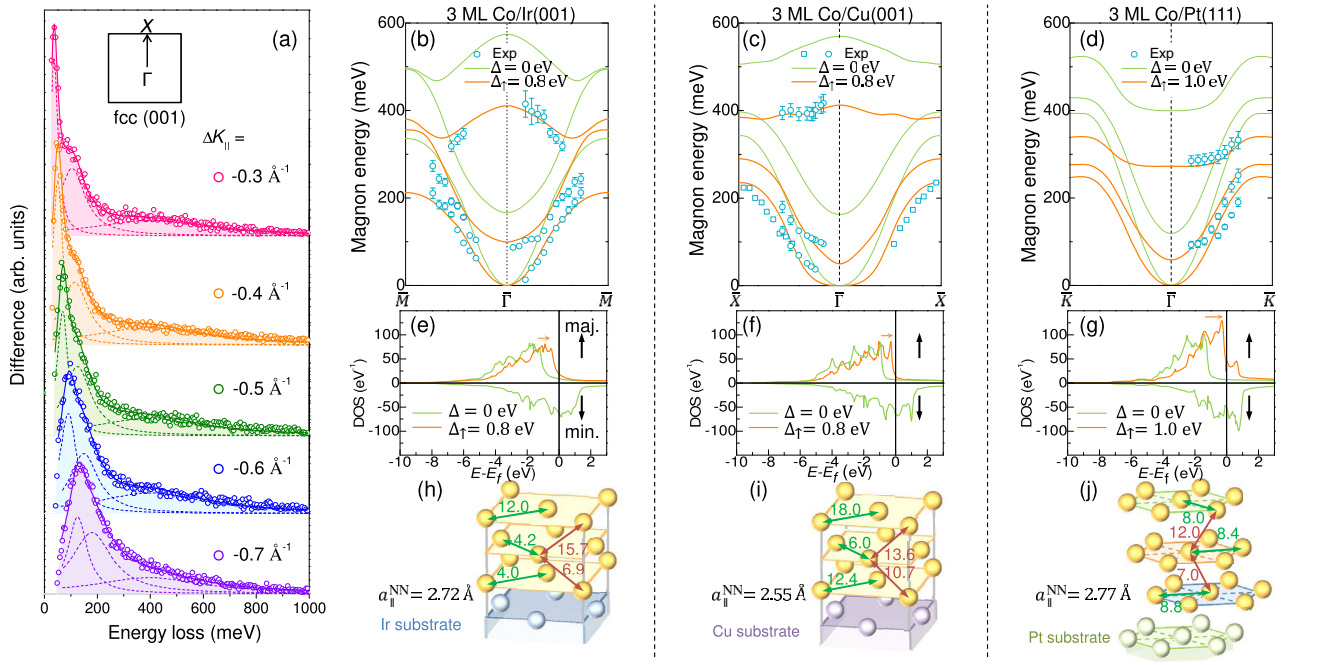

FIG. 2. (a) SPEELS difference spectra recorded on 3 ML Co/Cu(001) with $q_{\parallel}$ ranging from -0.3 to -0.7 Å^{-1} along the $\bar{\Gamma}-\bar{X}$ direction, with a primary energy of $E_i = 8$ eV. Experimental data (open circles) are fitted (solid line) with three Lorenzian line shapes (dashed lines), corresponding to confined magnon modes $n = 0$, 1, and 2. (b)–(d) The calculated (solid lines) and measured (open blue symbols) magnon dispersion and (e)–(g) the spin-resolved density of states for 3 ML Co on Ir(001), Cu(001), and Pt(111). Experimental points for the $n = 0$ mode in (c) denoted by □ were adapted from Ref. [28] for comparison. Calculations are performed with (i) no energy renormalization of the majority and minority bands ($\Delta = 0$ eV, green lines), and (ii) with an energy renormalization of the majority bands towards the Fermi level ($\Delta_{\uparrow} \neq 0$, orange lines), while keeping the minority bands unchanged. (h)–(j) Interatomic exchange parameters in meV resulting from the calculations indicated by (ii). The in-plane interatomic nearest-neighbor distance for each system is given by $a_{\parallel}^{\mathrm{NN}}$. The error bars in (b)–(d) include the uncertainties given by the goodness of the fit.

[33], serving as input for self-consistent calculations of the electronic structures. The interatomic exchange constants were calculated by employing the magnetic force theorem, similarly implemented within a Green's function formalism [38]. The calculated magnon dispersion relation and the spin-resolved density of states (DOS) are presented as the green lines in Figs. 2(b)–2(d) and Figs. 2(e)–2(g), respectively. By comparing the experimental and theoretical results, we find that the theoretically calculated magnon dispersion relation agrees qualitatively well with the experimental results. However, the quantitative agreement between theory and experiment is not satisfactory. The calculated magnon energies are overestimated by up to 160 meV for the $n = 2$ mode. The significant overestimation of the theoretically calculated magnon energies cannot be explained by introducing artificial modifications of the in- or out-of-plane lattice constants, film thickness, or surface reconstruction. It is well known that calculated magnon energies and exchange parameters are typically overestimated [14,26,39–42]. For instance, the magnon energies of 3 ML Co/Cu(001) predicted by first-principles calculations combined with atomistic spin dynamics simulations are higher than the experimental results by 260 meV [39].

It has been shown that the experimentally probed electronic band structures of Co films cannot be described adequately within the single-particle DFT [43,44]. A better agreement with experimental results is found by a renormalization of the majority-spin states of $3d$ bands towards the Fermi level, keeping the minority-spin states unchanged [43–45]. This observation has been attributed to the stronger correlation effects for the majority-spin states. It is therefore expected that the theory which can mimic many-body correlation effects shall predict a smaller value for the exchange splitting, compared to the values predicted by single-particle DFT-based approaches [43,44]. In order to mimic the spin-dependent many-body correlation effects on the dispersion relation of confined magnon modes, we performed the following calculations [see Figs. 2(e)–2(g)]: (i) no energy renormalization of the majority and minority bands is considered (the green lines indicated by $\Delta = 0$) and (ii) the majority bands are shifted towards the Fermi level (the orange lines indicated by $\Delta \neq 0$), while the minority bands are kept unchanged. The results of magnon dispersion and DOS are compared in Figs. 2(b)–2(d) and Figs. 2(e)–2(g), respectively. As only the energy of majority bands is renormalized in our calculations, the magnitude of this renormalization Δ directly corresponds to the reduction of the exchange splitting. Consequently, this leads to a reduction of the overestimated magnon energies.

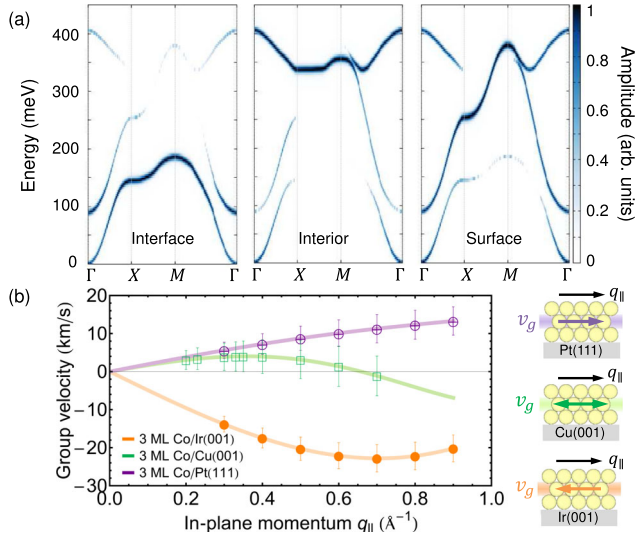

FIG. 3. (a) The calculated layer-resolved spectral function of the transverse susceptibility projected onto the interface, interior, and surface layers for 3 ML Co/Ir(001). The normalized amplitude of the spectral function is represented by the color bar. (b) Group velocity v_g as a function of $q_\parallel$ for the $n = 2$ mode of Co/Ir(001) (•), Co/Cu(001) (□), and Co/Pt(111) (⊕). The solid lines are a guide for the eye. (Insets) The relative direction between v_g and $q_\parallel$ (the same direction as the phase velocity of magnons).

As shown in Figs. 2(b)–2(d), for the best quantitative agreement with the experimental data, one needs to shift the majority bands (the up arrow) by $\Delta = 0.8$ eV towards the Fermi level (the orange line) for Co/Ir and Co/Cu, while the minority bands (the down arrow) are not changed (the green line). This renormalization of the majority-spin states in Co agrees surprisingly well with the experimental and theoretical results obtained by photoemission studies (a renormalization of 0.7–1.0 eV is reported as a result of the correlation effects) [43,44]. Note that one needs a slightly larger shift of $\Delta = 1.0$ eV for Co/Pt in order to explain the experimental data very well. Interestingly, the splitting between the highest majority- and minority-spin states of Co d bands for Co/Pt is 1.06 eV, in good agreement with the reported value of 1.05 eV found using photoemission experiments [46]. Our results highlight a strong correlation-induced renormalization of about 30% in the energies of the $n = 2$ magnon mode.

By comparing the experimental and theoretical magnon dispersion relations, the effective interatomic exchange interaction is quantitatively determined for all systems and the results are shown in Figs. 2(h)–2(j). The calculated interatomic exchange interaction of Co films are generally overestimated by DFT-based calculations [21,47]. We highlight a reduction of 25%–45% of the nearest-neighbor exchange constant, as compared with the results of calculations reported in the literature [39,41,42]. Our results imply that spin-dependent correlation effects play a decisive role in determining interatomic exchange interactions in such ultrathin elemental ferromagnets.

In principle, for a 3 ML ferromagnetic film on a substrate, the bonding environment for atoms situated at surface, interior, and interface layers is entirely different. Therefore, each magnon mode contains different contributions from the interface, interior, and surface layers (layer-specific localization of three magnon modes). In order to specify the contribution of each layer to the observed confined magnon modes, the layer-resolved spectral function of the transverse susceptibility of all magnon modes is shown in Fig. 3(a) for 3 ML Co/Ir(001). The magnetic moments located at the interface provide a dominant contribution to the $n = 0$ magnon mode. The $n = 1$ magnon mode has the largest amplitude at the surface and the $n = 2$ mode is localized at the middle layer, as similarly derived from a simple Heisenberg model [34]. A similar tendency of layer-specific localization is observed for Co/Cu(001) and Co/Pt(111) [34].

The group velocity is given by the gradient of the dispersion relation, i.e., $v_g = \partial_{q_\parallel} E(q_\parallel)$. The different dispersion curves of the $n = 2$ magnon mode [see Figs. 2(b)–2(d)] indicate the dramatically different propagation characteristics of the excited magnon wave packets, stemming from the changes in the sign (and also the magnitude) of v_g. Figure 3(b) presents the derived group velocities of the $n = 2$ mode for a 3 ML Co film on different substrates. Interestingly, for Co/Ir(001) the unusual "downward" dispersion of the $n = 2$ mode reflects the fact that the corresponding magnon wave packet exhibits a *negative* group velocity. As a result, the magnon wave packet propagates along a direction opposite that of $q_\parallel$, which is defined by the scattering geometry. We find that the sign of v_g of the $n = 2$ mode in the case of Co/Ir(001) is opposite that of Co/Pt(111). By contrast, for Co/Cu(001) the group velocity of the $n = 2$ mode is rather small and changes its sign with $q_\parallel$, being positive at low wave vectors and negative at high wave vectors.

In our first-principles calculations, we find a downward parabolic shape of the dispersion with negative group velocity when the interlayer distance of the Co layers changes from 1.92 to 1.61 Å, corresponding to a face-centered-cubic (fcc) and face-centered tetragonal film structure. Moreover, the ratio of the inter- ($J_\perp$) and intralayer ($J_\parallel$) exchange parameters increases by a factor of 2. This is the essential element for achieving the negative group velocity of the $n = 2$ magnon mode [34] and is a direct consequence of the tetragonally distorted lattice of the Co film grown on Ir(001) [29].

Previous studies have reported a negative v_g value of backward-volume dipolar magnons [48,49]. However, those magnons live in the gigahertz regime and on micrometer scales. As $q_\parallel$ increases, the dominating interaction of magnons varies from the magnetic dipole-dipole interaction to the much stronger and short-range exchange interaction. According to results presented in Fig. 3(a) for 3 ML Co/Ir(001), the terahertz confined magnon mode with

$n = 2$ is localized in the interior atomic layer and propagates in a direction opposite to that of the interface and surface magnon modes ($n = 0$ and 1). This means that it is an *exchange-dominated backward-volume mode* resulting from quantum confinement.

In summary, by tuning the structural properties of ultrathin Co films via growth on different substrates, we obtain inherently different in-plane magnon dispersions. This can even lead to an reversal of the group velocity of distinct magnon modes localized in adjacent atomic layers of a thin film, in the absence of external magnetic fields. Moreover, spin-dependent many-body correlations are shown to have a crucial impact on the dispersion relation of these terahertz magnon modes and the strength of the exchange interaction. Our findings provide an explanation for the long-standing problem of significant overestimation of theoretically calculated magnon energies and interatomic exchange energies in cobalt. Probing the confined magnon modes can open a way of estimating the effects of many-body correlations on the electronic band structures in ultrathin ferromagnets.

Y.-J. C thanks Christian Tusche for fruitful discussions on spin-dependent many-body correlation effects in Co thin films and Tzu-Hung Chuang for help with the initial stage of the experiments. Kh. Z. acknowledges funding from the Deutsche Forschungsgemeinschaft (DFG) through the Heisenberg Programme ZA 902/3-1 and DFG Grant No. ZA 902/4-1. A. E. acknowledges funding from the Deutsche Forschungsgemeinschaft (DFG priority program SPP 1538 "Spin Caloric Transport"). The calculations were performed at the Rechenzentrum Garching of the Max Planck Society (Germany).

*ying-jiun.chen@uni-due.de
Present address: Forschungszentrum Jülich, Peter Grünberg Institut PGI-6, 52425 Jülich, Germany and Fakultät für Physik, Universität Duisburg-Essen, 47057 Duisburg, Germany.
†khalil.zakeri@partner.kit.edu

[1] A. Khitun, M. Bao, and K. L. Wang, J. Phys. D **43**, 264005 (2010).
[2] M. Krawczyk and D. Grundler, J. Phys. Condens. Matter **26**, 123202 (2014).
[3] A. V. Chumak, V. I. Vasyuchka, A. A. Serga, and B. Hillebrands, Nat. Phys. **11**, 453 (2015).
[4] K. Ando and E. Saitoh, Nat. Commun. **3**, 629 (2012).
[5] T. Wakamura, H. Akaike, Y. Omori, Y. Niimi, S. Takahashi, A. Fujimaki, S. Maekawa, and Y. Otani, Nat. Mater. **14**, 675 (2015).
[6] J. Wunderlich, A. C. Irvine, J. Sinova, B. G. Park, L. P. Zarbo, X. L. Xu, B. Kaestner, V. Novak, and T. Jungwirth, Nat. Phys. **5**, 675 (2009).
[7] K. Uchida, H. Adachi, D. Kikuchi, S. Ito, Z. Qiu, S. Maekawa, and E. Saitoh, Nat. Commun. **6**, 5910 (2015).
[8] S. Sim, H. Jang, N. Koirala, M. Brahlek, J. Moon, J. H. Sung, J. Park, S. Cha, S. Oh, M.-H. Jo *et al.*, Nat. Commun. **6**, 8814 (2015).
[9] K.-S. Lee, D.-S. Han, and S.-K. Kim, Phys. Rev. Lett. **102**, 127202 (2009).
[10] M. I. Makin, J. H. Cole, C. D. Hill, and A. D. Greentree, Phys. Rev. Lett. **108**, 017207 (2012).
[11] A. Khitun, J. Appl. Phys. **111**, 054307 (2012).
[12] A. Khitun, J. Appl. Phys. **113**, 164503 (2013).
[13] X. Xing, Q. Jin, and S. Li, New J. Phys. **17**, 023020 (2015).
[14] T. Balashov, P. Buczek, L. Sandratskii, A. Ernst, and W. Wulfhekel, J. Phys. Condens. Matter **26**, 394007 (2014).
[15] K. Zakeri, T.-H. Chuang, A. Ernst, L. M. Sandratskii, P. Buczek, H. J. Qin, Y. Zhang, and J. Kirschner, Nat. Nanotechnol. **8**, 853 (2013).
[16] P. Buczek, A. Ernst, and L. M. Sandratskii, Phys. Rev. Lett. **105**, 097205 (2010).
[17] C. L. Gao, A. Ernst, G. Fischer, W. Hergert, P. Bruno, W. Wulfhekel, and J. Kirschner, Phys. Rev. Lett. **101**, 167201 (2008).
[18] J. Rajeswari, H. Ibach, C. M. Schneider, A. T. Costa, D. L. R. Santos, and D. L. Mills, Phys. Rev. B **86**, 165436 (2012).
[19] J. Rajeswari, Ph.D. thesis, University of Duisburg-Essen, 2013.
[20] H. Ibach, Surf. Sci. **630**, 301 (2014).
[21] J. Rajeswari, H. Ibach, and C. M. Schneider, Phys. Rev. Lett. **112**, 127202 (2014).
[22] E. Michel, H. Ibach, and C. M. Schneider, Phys. Rev. B **92**, 024407 (2015).
[23] R. Vollmer, M. Etzkorn, P. S. A. Kumar, H. Ibach, and J. Kirschner, Phys. Rev. Lett. **91**, 147201 (2003).
[24] K. Zakeri, Phys. Rep. **545**, 47 (2014).
[25] Y. Zhang, T.-H. Chuang, K. Zakeri, and J. Kirschner, Phys. Rev. Lett. **109**, 087203 (2012).
[26] H. J. Qin, K. Zakeri, A. Ernst, T.-H. Chuang, Y.-J. Chen, Y. Meng, and J. Kirschner, Phys. Rev. B **88**, 020404 (2013).
[27] D. W. Marquardt, J. Soc. Ind. Appl. Math. **11**, 431 (1963).
[28] M. Etzkorn, P. A. Kumar, R. Vollmer, H. Ibach, and J. Kirschner, Surf. Sci. **566–568**, 241 (2004).
[29] K. Heinz and L. Hammer, Prog. Surf. Sci. **84**, 2 (2009).
[30] Z. Tian, D. Sander, and J. Kirschner, Phys. Rev. B **79**, 024432 (2009).
[31] O. Heckmann, H. Magnan, P. le Fevre, D. Chandesris, and J. Rehr, Surf. Sci. **312**, 62 (1994).
[32] C. M. Schneider, P. Bressler, P. Schuster, J. Kirschner, J. J. de Miguel, and R. Miranda, Phys. Rev. Lett. **64**, 1059 (1990).
[33] S. M. Valvidares, J. Dorantes-Dávila, H. Isern, S. Ferrer, and G. M. Pastor, Phys. Rev. B **81**, 024415 (2010).
[34] See Supplemental Material at http://link.aps.org/supplemental/10.1103/PhysRevLett.119.267201, which includes Refs. [29–33], for detailed information.
[35] J. P. Perdew, K. Burke, and M. Ernzerhof, Phys. Rev. Lett. **77**, 3865 (1996).
[36] M. Lüders, A. Ernst, W. M. Temmerman, Z. Szotek, and P. J. Durham, J. Phys. Condens. Matter **13**, 8587 (2001).
[37] J. R. Cerda, P. L. de Andres, A. Cebollada, R. Miranda, E. Navas, P. Schuster, C. M. Schneider, and J. Kirschner, J. Phys. Condens. Matter **5**, 2055 (1993).

[38] A. Liechtenstein, M. Katsnelson, V. Antropov, and V. Gubanov, J. Magn. Magn. Mater. **67**, 65 (1987).
[39] A. Taroni, A. Bergman, L. Bergqvist, J. Hellsvik, and O. Eriksson, Phys. Rev. Lett. **107**, 037202 (2011).
[40] T.-H. Chuang, K. Zakeri, A. Ernst, L. M. Sandratskii, P. Buczek, Y. Zhang, H. J. Qin, W. Adeagbo, W. Hergert, and J. Kirschner, Phys. Rev. Lett. **109**, 207201 (2012).
[41] L. Bergqvist, A. Taroni, A. Bergman, C. Etz, and O. Eriksson, Phys. Rev. B **87**, 144401 (2013).
[42] A. T. Costa, R. B. Muniz, and D. L. Mills, Phys. Rev. B **69**, 064413 (2004).
[43] S. Monastra, F. Manghi, C. A. Rozzi, C. Arcangeli, E. Wetli, H.-J. Neff, T. Greber, and J. Osterwalder, Phys. Rev. Lett. **88**, 236402 (2002).
[44] J. Sánchez-Barriga, J. Minár, J. Braun, A. Varykhalov, V. Boni, I. Di Marco, O. Rader, V. Bellini, F. Manghi, H. Ebert *et al.*, Phys. Rev. B **82**, 104414 (2010).
[45] J. Sánchez-Barriga, J. Braun, J. Minár, I. Di Marco, A. Varykhalov, O. Rader, V. Boni, V. Bellini, F. Manghi, H. Ebert *et al.*, Phys. Rev. B **85**, 205109 (2012).
[46] M. Mulazzi, J. Miyawaki, A. Chainani, Y. Takata, M. Taguchi, M. Oura, Y. Senba, H. Ohashi, and S. Shin, Phys. Rev. B **80**, 241106 (2009).
[47] M. Pajda, J. Kudrnovský, I. Turek, V. Drchal, and P. Bruno, Phys. Rev. B **64**, 174402 (2001).
[48] A. V. Chumak, P. Dhagat, A. Jander, A. A. Serga, and B. Hillebrands, Phys. Rev. B **81**, 140404 (2010).
[49] P. Wessels, A. Vogel, J.-N. Tödt, M. Wieland, G. Meier, and M. Drescher, Sci. Rep. **6**, 22117 (2016).